LBL-38233
UC-402
Preprint

Lawrence Berkeley Laboratory

UNIVERSITY OF CALIFORNIA

ENERGY & ENVIRONMENT DIVISION

Submitted to Atmospheric Environment

Soil-Gas Entry into Houses Driven by Atmospheric Pressure Fluctuations, Part 2—The Influence of Soil Properties

A.L. Robinson, R.G. Sextro, and W.J. Riley

February 1996

ENERGY
AND ENVIRONMENT
DIVISION

REFERENCE COPY
Does Not
Circulate
Bldg. 50 Library.
LBL-38233
Copy 1

Prepared for the U.S. Department of Energy under Contract Number DE-AC03-76SF00098

DISCLAIMER

This document was prepared as an account of work sponsored by the United States Government. While this document is believed to contain correct information, neither the United States Government nor any agency thereof, nor the Regents of the University of California, nor any of their employees, makes any warranty, express or implied, or assumes any legal responsibility for the accuracy, completeness, or usefulness of any information, apparatus, product, or process disclosed, or represents that its use would not infringe privately owned rights. Reference herein to any specific commercial product, process, or service by its trade name, trademark, manufacturer, or otherwise, does not necessarily constitute or imply its endorsement, recommendation, or favoring by the United States Government or any agency thereof, or the Regents of the University of California. The views and opinions of authors expressed herein do not necessarily state or reflect those of the United States Government or any agency thereof or the Regents of the University of California.

Submitted to *Atmospheric Environment*

LBL-38233
UC-402

Soil-Gas Entry into Houses Driven by Atmospheric Pressure Fluctuations, Part 2 --- The Influence of Soil Properties

Allen L. Robinson, Richard G. Sextro, William J. Riley

February 1996

Indoor Environment Program
Energy and Environment Division
Lawrence Berkeley National Laboratory
1 Cyclotron Road
Berkeley, CA 94720

This work was supported by the Director, Office of Energy Research, Office of Health and Environmental Research, Environmental Sciences Division, and by the Assistant Secretary for Energy Efficiency and Renewable Energy, Office of Building Technology of the U.S. Department of Energy (DOE), under Contract DE-AC03-76SF00098.

ABSTRACT

Atmospheric pressure fluctuations can draw soil gas into houses without the indoor-outdoor pressure differences commonly associated with the advective entry of radon and other soil-gas contaminants. To investigate the influence of soil properties, water table depth, and a high-permeability subslab gravel layer on this phenomenon, we employ a finite-element model to simulate the soil-gas flow around a basement caused by changes in atmospheric pressure. The characteristic response time and the capacitance of the soil are used to characterize how changes in permeability, air-filled porosity, and water table depth affect this soil-gas flow. The shorter the characteristic response time and the larger the capacitance of the soil, the larger the soil-gas flow rate caused by a given fluctuation in atmospheric pressure. Relative to entry driven by steady indoor-outdoor pressure differences, contaminant entry driven by atmospheric pressure fluctuations will likely be most important in houses situated in a soil of low permeability ($< 10^{-12}$ m^2) and large air-filled porosity.

Key word index: radon, atmospheric pressure, indoor-air quality, contaminant transport, soil-gas transport

INTRODUCTION

Soil-gas entry into houses has been studied in relation to indoor exposures of humans to radon progeny and volatile organic chemicals (VOCs). Advective entry of radon-bearing soil gas is generally believed to be the dominant transport mechanism of radon into most homes with elevated indoor concentrations (see review by Nazaroff (1992)). Advective soil-gas flow may also be an important transport mechanism of VOCs and methane into houses built near landfills or leaky gasoline storage tanks (Hodgson et al., 1992; Little et al., 1992).

Most investigations of soil-gas entry into houses have focused on entry driven by slight (a few Pa) but persistent indoor-outdoor pressure difference (see review by Nazaroff (1992)). The phrase "indoor-outdoor pressure difference" refers to the pressure difference between the ambient atmosphere at the soil surface and the indoor air at an opening between the basement and the soil. Recent theoretical (Narasimhan et al., 1990; Tsang and Narasimhan, 1992) and experimental studies (Robinson and Sextro, 1995a; Robinson et al., 1996) indicate that changes in atmospheric pressure can draw soil gas into a building in the absence of these persistent indoor-outdoor pressure differences.

In this two part study, we present a detailed examination of the gas flow between a building and the underlying soil in response to changes in atmospheric pressure. The goal of this study is to characterize the relationship between this flow, soil properties, and typical atmospheric pressure fluctuations. A thorough understanding of this transient gas flow is an important step towards understanding the complex effect of atmospheric pressure fluctuations on the entry of radon and other soil-gas contaminants into buildings.

In the first part of this study (Robinson *et al.*, 1996), we examined measurements of atmospheric pressure and gas flow into and out of an experimental basement structure. The characteristic response time of the soil and the time-rate-of-change of the atmospheric pressure signal play important roles in determining the soil-gas flow rate into the experimental structure. To build on this understanding, this paper reports on a parametric investigation into the influence of soil properties, water table depth, and a high-permeability subslab gravel layer on soil-gas entry into houses. We derive a set of parameters which can be used to estimate the gas flow rate into and out of a building in response to changes in atmospheric pressure. We employ a transient finite-element model to demonstrate how these parameters influence this flow. In the first part of this study, this finite-element model correctly predicted the observed gas flow rate into and out of an experimental basement caused by changes in atmospheric pressure.

METHODS

We employ the following algorithm to examine the effect of typical atmospheric pressure fluctuations on gas flow into and out of a basement. First, we calculate the soil-gas flow into a prototypical basement caused by a unit-step change in atmospheric pressure using a finite-element model. These predictions are then transformed into the frequency domain and combined with an estimate of the long-term atmospheric pressure power spectrum to estimate the rate at which typical atmospheric pressure fluctuations pump gas into and out of a basement. Two scaling

parameters derived from a previously reported analytical model (Robinson and Sextro, 1995a; Robinson *et al.*, 1996) are used to interpret the calculated long-term soil-gas flow rates.

Spectral analysis of atmospheric pressure data

The atmospheric pressure data reported in this paper have been collected in conjunction with an ongoing experimental investigation of soil-gas and radon entry into buildings (e.g. Fisk et al., 1992; Garbesi et al., 1993; Robinson and Sextro, 1995b). To characterize typical atmospheric pressure fluctuations, we calculated the power spectra of the measured atmospheric pressure and time-rate-of-change of atmospheric pressure. For this analysis we employed the algorithm described by Bendat and Piersol (Bendat and Piersol, 1986); a brief description of this algorithm is found in the first part of this study (Robinson *et al.*, 1996). To estimate the power spectrum at low-frequencies (< 50 day^{-1}), we analyzed 18-day-long blocks of continuous atmospheric pressure measurements made at 2 min intervals. These data were drawn from 108 days of non-sequential atmospheric pressure measurements collected in 1993. To estimate the power spectrum at high frequencies (> 25 day^{-1}), we analyzed 48-hour-long blocks of continuous atmospheric pressure data collected at 5-s intervals. These data were drawn from 15 days of non-sequential atmospheric pressure measurements collected in fall of 1994. These estimates were combined by averaging the values in the overlapping frequency bins.

House Substructure and Soil Properties

The geometry of the model basement shell and the surrounding soil is shown in Fig. 1. As Fig. 1a indicates, we have defined our prototypical basement as a cylinder surrounded by a cylindrical soil block. By defining such a basement and utilizing an axial-symmetric radial coordinate system we significantly reduce the computational requirements of the model while preserving the basement's volume and floor area. Although real houses have rectangular basements, we expect that the results of this study are directly applicable to real houses. Revzan et al. (1991) compared predictions of steady-state soil-gas entry using a cylindrical model with those generated with a three-dimensional Cartesian model and found no significant discrepancy for houses which are symmetric in the vertical plane. In the first part of this study (Robinson *et al.*, 1996), the transient cylindrical model correctly predicted the observed gas flow into and out of a rectangular experimental basement in response to changes in atmospheric pressure.

Two different basement configurations were examined: a dirt floor, and a concrete slab with a perimeter crack. The perimeter crack is a 1-cm-wide gap around the edge of the slab floor. Such an opening simulates the shrinkage gap that can develop at the floor-wall joint located at the perimeter of the poured concrete floor in real houses. Although the opening considered in this study is wider than the shrinkage gap found in typical houses (Scott, 1988), we have used this opening size to eliminate crack resistance from the problem, which permits a focused analysis into the influence of soil properties on soil-gas entry. However, we expect that the impedance of the soil-structure system to soil-gas flow will largely be determined by the properties of the soil; therefore, more realistic crack configurations will probably not significantly affect on this flow.

Two different sets of simulations were run to examine the sensitivity of the soil-gas entry rate to changes in soil permeability, air-filled porosity, and water table depth. As Fig. 1b indicates, the water table depth is the vertical distance between the basement floor and the water table, bedrock, or some other impermeable layer. Tables 1 and 2 list the values of these properties used for each set of simulations. These values reflect the range of soils in which houses are commonly found (Bear, 1972; Nazaroff, 1992). For most of the cases studied we have assumed a homogeneous soil block. The only heterogeneity considered in this study is a high permeability subslab gravel layer. A subslab gravel layer is a common construction practice in many areas as a means of preventing the concrete floor slab from coming into contact with wet soil. It has been found to significantly increase soil-gas entry driven by steady indoor-outdoor pressure differences (Revzan and Fisk, 1992; Robinson and Sextro, 1995b). We assigned the gravel layer an air-filled porosity of 0.3, and varied its permeability between 10^{-8} and 10^{-11} m^2.

Q_{RMS} as an Indicator for Contaminant Entry

Although the long-term soil-gas entry rate driven by atmospheric pressure fluctuations is zero, transient gas flow into and out of a house can cause a net contaminant entry rate into a house because of the difference between the concentration of a contaminant in indoor air and its concentration in the soil gas underneath a concrete floor slab (Tsang and Narasimhan, 1992; Robinson *et al.*, 1996). Unfortunately, the relationship between soil-gas flow driven by atmospheric pressure fluctuations and the transport of soil-gas contaminants into houses is unknown. Detailed analysis of this relationship is difficult due to dilution of contaminant concentrations in the soil underneath a basement by the outflow of low-concentration indoor air in response to rising atmospheric pressure.

In order to examine the effect of atmospheric pressure fluctuations on contaminant entry, we will characterize the long-term gas flow rate into and out of house in terms of the root-mean-square soil-gas flow rate, Q_{RMS} ($m^3\ s^{-1}$). Q_{RMS} is a measure of the volume of gas being pumped into and out of a building by changes in atmospheric pressure. We expect that the larger this volume the larger the contaminant entry rate; therefore, Q_{RMS} can act as a surrogate for contaminant entry.

The mean-square soil-gas flow rate, Q^2_{RMS} , is defined as

$$Q^2_{RMS} = \frac{1}{T}\int_0^T q^2(t)dt \qquad (1)$$

where q(t) is the time-dependent gas flow rate into and out of a building driven by atmospheric pressure fluctuations ($m^3\ s^{-1}$). The period over which the average is taken, T (s), must be large enough so that the average soil-gas entry rate is zero. If T is much longer than the characteristic time of typical atmospheric pressure fluctuations then Q_{RMS} quantifies the average rate at which gas is being pumped into and out of building. As T approaches infinity, we can use Parseval's Theorem to define Q_{RMS} in the frequency domain (Bendat and Piersol, 1986)

$$Q^2_{RMS} = \lim_{T\to\infty} \frac{1}{T}\int_0^T q^2(t)dt = \int_0^\infty f_q(\omega)d\omega, \qquad (2)$$

where $f_q(\omega)$ is the soil-gas flow power spectrum ($m^6\ s^{-1}$), and ω is the circular frequency (radians s^{-1}).

For this paper, we have evaluated Q_{RMS} in the frequency domain using eqn. (2). This evaluation requires an estimate of the soil-gas flow power spectrum, $f_q(\omega)$. We briefly describe some of the equations necessary to calculate $f_q(\omega)$. A more complete description of the theory used to describe soil-gas flow driven by atmospheric pressure fluctuations can be found in the first part of this study (Robinson *et al.*, 1996).

Since the equation which governs soil-gas flow induced by changes in atmospheric pressure is linear, this flow can be characterized in either the time or the frequency domains. In the time domain, q(t) is defined in terms of the step response function,

$$q(t) = \int_{-\infty}^{t} Q_{step}(t-\theta)\, P'_{atm}(\theta) d\theta \tag{3}$$

where P'_{atm} is the time-rate-of-change of the atmospheric pressure (Pa s^{-1}), and θ is the dummy variable for integration over time (s). The step response function, $Q_{step}(t)$ ($m^3\ s^{-1}\ Pa^{-1}$), defines the soil-gas entry rate caused by a 1 Pa step change in atmospheric pressure.

In the frequency domain, q(t) is characterized by the frequency response function, $\chi(\omega)$ ($m^3\ Pa^{-1}$), which is defined as the Fourier transform of $Q_{step}(t)$

$$\chi(\omega) = \int_{0}^{\infty} Q_{step}(\theta)\, e^{-i\omega\theta} d\theta. \tag{4}$$

The complex-valued frequency response function is generally reported in terms of the gain and phase functions,

$$G_{q,dp}(\omega) = |\chi(\omega)| \tag{5a}$$

$$\phi_{q,dp}(\omega) = \arg(\chi(\omega)) \tag{5b}$$

where arg( ) and | | define the argument and modulus of a complex number, respectively. The gain function, $G_{q,dp}(\omega)$ ($m^3\ Pa^{-1}$), defines the amplitude of q(t) caused by an oscillation in the time-rate-of-change of atmospheric pressure as a function of frequency. The phase function, $\phi_{q,dp}(\omega)$ (radians), defines the phase lag between q(t) and an oscillation in the time-rate-of-change in atmospheric pressure as a function of frequency.

By taking the Fourier transform of eqn. (3) and utilizing the definition of $\chi(\omega)$ we can express the soil-gas flow power spectrum, $f_q(\omega)$, as (Chatfield, 1989)

$$f_q(\omega) = G^2_{q,dp}(\omega)\, f_{dp}(\omega) \tag{6}$$

where $f_{dp}(\omega)$ is the time-rate-of-change of atmospheric pressure power spectrum ($Pa^2\ s^{-1}$).

Evaluating Q_{RMS} in the frequency domain using eqns. (2) and (6) requires substantially fewer calculations then an evaluation of Q_{RMS} in the time domain. To analyze different soil and basement configurations in the frequency domain requires that we determine the frequency response function for each configuration. Each of these frequency response functions can be combined with one estimate of $f_{dp}(\omega)$. In contrast, analysis in the time domain requires evaluation of several weeks of atmospheric pressure data for each of the different soil/basement configurations.

Description of Numerical Simulations

We employ a finite-element model to calculate $Q_{step}(t)$ and the steady-state soil-gas entry rate caused by a 1 Pa indoor-outdoor pressure difference for the different combinations of soil properties and basement configurations. The model calculates the soil-gas flow rate into the basement by simulating the soil-gas pressure and velocity fields in the region shown in Fig. 1b. This flow rate is determined by integrating the soil-gas velocity normal to the opening in the basement floor. The finite-element code is based on the RN3D model written by Holford (1994). The model treats the soil gas as an ideal gas, and assumes that its flow is governed by Darcy's Law. More details on our use of this model are found in the first part of this study (Robinson *et al.*, 1996).

The following initial and boundary conditions are used to calculate $Q_{step}(t)$: initially ($t = 0$ s) the entire soil block is defined to have a pressure of 100,000 Pa; for $t > 0$ s the soil surface (indicated as P1 in Fig. 1b) and the mouth of the opening in the basement floor (indicated as P2 in Fig. 1b) are assigned a pressure of 99,999 Pa. As Fig. 1b indicates, the outside edge of the concrete walls, floor, and footer are defined as no-flow boundaries. The bottom of the soil block is defined as a no-flow boundary which physically represents a water table, bedrock, or some other impermeable layer. The outside edge of the soil block is also defined as a no-flow boundary. The radius of the soil block (20 m) was chosen such that the outside edge of the soil block falls outside the domain of influence of the structure.

To evaluate $Q_{step}(t)$, the model predicts the evolution of the soil-gas pressure and velocity fields using a fully-implicit time discretization scheme. The simulation is ended when the flow rate into the basement has fallen 7 orders of magnitude from its peak value. At this point, we assume that the soil gas and atmospheric pressure have reached equilibrium. In addition, we assume that changes in atmospheric pressure are communicated instantaneously to the interior of the basement, that the atmospheric pressure is uniform across the entire soil surface, and that the opening in floor creates no resistance to gas flow. To evaluate Q_{RMS}, we transform $Q_{step}(t)$ into the frequency domain by numerically integrating eqn. (4).

To compare the soil-gas flow rate into a basement caused by a change in atmospheric pressure to the entry rate caused by a steady indoor-outdoor pressure difference, we also used the finite-element model to predict the steady-state soil-gas entry rate induced by a 1 Pa indoor-outdoor pressure difference, Q_{SS}. For this analysis, the model calculates the steady-state soil-gas pressure and velocity fields for the region shown in Fig. 1b in response to the following boundary conditions: the pressure at the soil surface (indicated as P1 in Fig. 1b) is defined as 100,000 Pa

and the pressure at the mouth of the opening in the basement floor (indicated as P2 in Fig. 1b) is defined as 99,999 Pa. As previously described, all of the other boundaries of the soil block are treated as no-flow.

Description of Analytical Model

In this section we reproduce the analytical model derived in the first part of this study (Robinson *et al.*, 1996). We employ this model to interpret the predictions of the numerical model. The step response function, $Q_{step}(t)$, defined by the analytical model is

$$Q_{step}(t) = \frac{k}{\mu}\frac{2}{L}A\sum_{n=0}^{\infty}\exp\left(-\frac{t}{T_n}\right) \qquad \text{for } t \geq 0. \tag{7}$$

The frequency response function, $\chi_a(\omega)$, defined by the analytical model is

$$\chi_a(\omega) = \frac{8}{\pi^2}\frac{L\varepsilon}{\overline{P}}A\sum_{n=0}^{\infty}\frac{1}{(2n+1)^2}\frac{1-i\omega T_n}{1+(\omega T_n)^2}, \qquad \text{for } \omega > 0. \tag{8}$$

where k indicates soil permeability to air (m^2), μ is the dynamic viscosity of the soil gas (Pa s), A is the cross-sectional area of the floor slab (m^2), ε is the air-filled porosity (-), $\overline{P}$ is the mean soil-gas pressure (Pa), and $T_n = \frac{1}{(2n+1)^2}\left(\frac{4}{\pi^2}\right)\left(\frac{L^2\varepsilon\mu}{k\overline{P}}\right)$ (s). L is the distance between the basement floor and the water table, bedrock or some other impermeable layer (m). For convenience, we will refer to L as the water table depth.

RESULTS AND DISCUSSION

Typical Atmospheric Pressure Fluctuations

To illustrate the magnitude and frequency of typical atmospheric pressure fluctuations, 24 days of continuous atmospheric pressure data are shown in Fig. 2. Diurnal heating of the earth's surface cause the prominent 200 Pa oscillations. Passing weather fronts can cause changes in pressure greater than 1000 Pa. Gossard and Hooke (1975) describe the variety of mechanisms that cause changes in atmospheric pressure.

The calculated time-rate-of-change of atmospheric pressure for this 24-day period is shown in Fig. 2b. Comparing Figs. 2a and 2b reveals that the largest time-rates-of-change correspond to relatively small, but rapid changes in pressure. The time-rates-of-change associated with the very large (> 1000 Pa) changes in atmospheric pressure are typically small because these changes generally occur over periods of days. The prominent diurnal and semi-diurnal oscillations shown in Fig. 2a cause ~ 1 Pa min^{-1} oscillations in the time-rate-of-change of atmospheric pressure.

The power spectra shown in Fig. 3a characterize typical changes in atmospheric pressure in the frequency domain. The first spectrum was calculated from 108 days of measured atmospheric pressure data and identifies the magnitude and frequency of typical fluctuations in atmospheric pressure. This spectrum is consistent with previously

reported atmospheric pressure power spectra (Gossard, 1960). The second spectrum, indicated by the dashed line in Fig. 3a, was calculated from a 5-hour period of atmospheric pressure data. It characterizes the magnitude and frequency of the relatively small, but rapid pressure fluctuations which create the largest time-rates-of-change of atmospheric pressure. The associated power spectra for the time-rate-of-change of atmospheric pressure are shown in Fig. 3b.

The long-term power spectra shown in Figs. 3a and 3b reveal several important characteristics of typical atmospheric pressure fluctuations. The prominent spikes occurring at frequencies of 1 and 2 day^{-1} indicate that diurnal and semi-diurnal oscillations are the dominant oscillations in atmospheric pressure. In addition, more than 60% of the total power of the long-term time-rate-of-change spectrum occurs at frequencies less than 100 day^{-1}. Comparing the short-term and long-term power spectra shown in Fig. 3b indicates that high-frequency pressure fluctuations can substantially increase the total power of the time-rate-of-change of atmospheric pressure. The short-term spectrum has 6 times more power than the long-term spectrum. However, the absence of a high-frequency peak in the long-term spectrum reveals that such fluctuations only occur intermittently. These high-frequency fluctuations also temporarily shift the distribution of power from low-frequencies to high-frequencies. For example, only 40% of the power of the short-term spectrum shown in Fig. 3b is at frequencies less than 100 day^{-1}.

Scaling parameters

The gas flow rate between a building and the underlying soil can be understood in terms of two scaling parameters derived through dimensional analysis of the analytical model, eqns. (7) and (8). Despite the many assumptions required for the derivation of this analytical model (Robinson *et al.*, 1996), predictions of the finite-element model indicate that these two parameters describe how q(t) scales with changes in air-filled porosity, permeability, and water table depth.

The first scaling parameter is the capacitance of the soil block. It characterizes the volume of soil gas that flows into a house in response to a step change in atmospheric pressure. The capacitance, C ($m^3\ Pa^{-1}$), can be defined as

$$C = \frac{L\varepsilon}{\overline{P}} A . \tag{9}$$

The second scaling parameter is the characteristic response time of the soil gas to changes in atmospheric pressure. Such a parameter can be defined based on the time for a pressure disturbance to propagate a characteristic length scale of the system;

$$\tau = \frac{L^2}{D_p} = \left(\frac{L\varepsilon}{\overline{P}}\right)\left(\frac{L\mu}{k}\right) = C \cdot R \tag{10}$$

where D_p is the pressure diffusivity of the soil gas ($D_p = \overline{P}k/\mu\varepsilon$) ($m^2\ s^{-1}$). The characteristic response time, τ (s), can be expressed as the product of the capacitance, C, and the resistance of the soil to gas flow, $R = L\mu/Ak$ ($Pa\ s\ m^{-3}$).

Values for these parameters for the different combinations of soil properties and water table depths considered in this study are listed in Tables 1 and 2. The characteristic response time of typical soils varies from seconds to days; the capacitance of typical soils varies between 1 and 10 L Pa^{-1}. Although the characteristic response time depends on the water table depth, air-filled porosity, and permeability, the calculations shown in Tables 1 and 2 indicate that the permeability determines the range of this response time because the permeability of common soils can span more than six orders of magnitude (10^{-9} - 10^{-15} m^2) (Nazaroff, 1992). In contrast, the air-filled porosity and water table depth typically vary within an order of magnitude.

The results presented in Fig. 4 illustrate the relationship between q(t) and these scaling parameters in the time domain. Fig. 4a shows the measured atmospheric pressure data used as the boundary condition for this analysis. The time-rate-of-change of this atmospheric pressure signal is shown in Fig. 4b. We examined the measured gas flow rate into and out of an experimental basement structure in response to this one-hour atmospheric pressure signal in the first part of this study (Robinson *et al.*, 1996). The results shown in Figs. 4c and 4d were calculated using $Q_{step}(t)$ for a dirt floor basement and eqn. (3). $Q_{step}(t)$ was evaluated with the numerical model; the soil properties used for these simulations are listed in Table 1. A comparison of the flow rates shown in Fig. 4c reveals that the magnitude of q(t) scales with the capacitance of the soil block. Comparing the flow rates shown in Fig. 4d indicates that the characteristic response time acts as a low-pass filter dampening q(t) at high-frequencies.

Unfortunately, the results shown in Fig. 4 reveal only qualitative aspects of the relationship between the scaling parameters and q(t). We can improve our understanding of this relationship by transforming our analysis into the frequency domain. The gain, $G_{q,dp}(\omega)$, and phase, $\phi_{q,dp}(\omega)$, functions shown in Fig. 5 describe q(t) as a function of the frequency of fluctuations in atmospheric pressure. $G_{q,dp}(\omega)$ defines the amplitude of q(t) caused by a 1 Pa min^{-1} oscillation in the time-rate-of-change of atmospheric pressure as a function of frequency --- the larger $G_{q,dp}(\omega)$, the larger q(t). $\phi_{q,dp}(\omega)$ defines the phase shift between an oscillation in the time-rate-of-change of atmospheric pressure and q(t). We calculated $G_{q,dp}(\omega)$ and $\phi_{q,dp}(\omega)$ by transforming the step response functions used for the analysis presented in Fig. 4 into the frequency domain.

The gain functions shown in Fig. 5a illustrate the effect of changing the capacitance of the soil on the magnitude of q(t) for a fixed value of the characteristic response time. As noted earlier, increasing the capacitance increases the volume of soil gas which is compressed and expanded with changes in atmospheric pressure. The estimates of $G_{q,dp}(\omega)$ shown in Fig. 5a indicate the magnitude of q(t) scales linearly with the capacitance. If the characteristic response time of the soil is held constant, changing the capacitance does not affect the spectral composition of q(t).

The estimates of $G_{q,dp}(\omega)$ shown in Fig. 5b provide insight into the relationship between the characteristic response time of the soil and the filtering of high-frequency fluctuations in atmospheric pressure. These results were calculated by changing this response time while holding the capacitance fixed. The roll-off of the gain function

occurs at the frequency where the finite response time of the soil gas begins to restrict the gas flow rate caused by high-frequency changes in atmospheric pressure --- the shorter the response time, the higher the roll-off frequency.

The phase lag between q(t) and the time-rate-of-change in atmospheric pressure further illustrates the relationship between the characteristic response time and q(t). In Fig. 5c we plot estimates of $\phi_{q,dp}(\omega)$. These estimates correspond to the gain functions shown in Figs. 5a and 5b. The phase shift only depends on the characteristic response time of the soil. Increasing this response time decreases the frequency at which the q(t) begins to lag the time-rate-of-change of atmospheric pressure.

The results in Fig. 5b suggest that for a fixed value of the capacitance, the gain function converges to the same value at low frequencies. This implies that q(t) driven by very low-frequency fluctuations in atmospheric pressure does not depend on the permeability of the soil. In light of the linear relationship between permeability and soil-gas entry driven by steady indoor-outdoor pressure differences this appears to be a surprising prediction. The low-frequency behavior of q(t) can be understood by examining the low-frequency limit of $\chi(\omega)$,

$$\lim_{\omega \to 0} \chi(\omega) = \int_0^\infty Q_{step}(\theta) d\theta. \tag{11}$$

Using eqns. (5a) and (5b) we can rewrite this limit in terms of the gain and phase functions,

$$\lim_{\omega \to 0} G_{q,dp}(\omega) = \int_0^\infty Q_{step}(\theta) d\theta, \text{ and} \tag{12a}$$

$$\lim_{\omega \to 0} \phi_{q,dp}(\omega) = 0. \tag{12b}$$

Eqn. (12a) reveals that the magnitude of q(t) driven by low-frequency fluctuations atmospheric pressure is defined by the volume of soil gas which flows into a basement in response to a step change in atmospheric pressure. At very low-frequencies, the period of the atmospheric pressure oscillations is many times longer than the characteristic response time of the soil. Consequently, the entire soil block completely responds to these fluctuations.

For a fixed water table depth, the two-scaling parameters derived from the analytical model predict exactly how changes in air-filled porosity and permeability interact to determine q(t). However, these parameters do not describe exactly how changes in water table depth affect q(t). We can examine this failure by plotting the low-frequency limit of $\chi(\omega)$ as a function of the capacitance. Ideally this relationship should be linear because eqn. (11) indicates that the low-frequency limit of $\chi(\omega)$ is a measure of the "true" capacitance (the capacitance characterizes the volume of soil gas which flows into a building in response to a step change in atmospheric pressure). Our expression for the capacitance, eqn. (9), does not exactly define this volume because the soil-gas flow around a basement in response to a change in atmospheric pressure is not one-dimensional (see streamline plot, Fig. 3, in the first part of this study (Robinson *et al.*, 1996)). Although Fig. 6 indicates that the low-frequency limit of $\chi(\omega)$ for a dirt floor basement does not scale linearly with capacitance, we can accurately approximate this relationship as linear. A linear

regression of the low frequency limit of $\chi(\omega)$ as a function of the capacitance yields an R^2 greater than 0.999 for the range of water table depths considered in this study.

Effect of a high-permeability subslab gravel layer

In this section, we explore the effect of a high-permeability subslab gravel layer on q(t) using the numerical model. The gain functions shown in Fig. 7a indicate that the addition of a subslab gravel layer increases the magnitude of q(t) for a basement with a small perimeter crack by more than a factor 3. The size of the increase depends on the ratio of the permeability of the gravel layer to that of the rest of the soil block.

The effect of a high permeability subslab gravel layer can be understood by comparing the characteristic response time of the gravel layer to the response time of the soil block. Since the permeability of gravel is typically orders of magnitude larger than that of common soils, the response time of a gravel layer to a change in pressure is orders of magnitude shorter than the rest of the soil block. Therefore, the gravel layer will respond instantaneously to changes in atmospheric pressure relative to the rest of the soil, effectively creating an isobaric plenum underneath the basement. The gain and phase functions shown in Fig. 7 indicate that if the permeability of this gravel layer is more than 2 orders of magnitude greater than that of the surrounding soil, the basement will essentially interact with the surrounding soil as if it had a dirt floor. Consequently, we will focus our examination on the two extremes, a basement with and without a floor slab.

Comparing the roll-off of the gain functions shown in Fig. 7a indicates that the addition of a high-permeability subslab gravel layer has little effect on the characteristic response time of the system. An examination of the calculated soil-gas velocity field around the basement reveals that a subslab gravel layer dramatically increases the size of the region from which a building draws soil gas. This, in effect, increases the capacitance of the system. The size of this region depends on the two-dimensional nature of the soil-gas flow field (for example see streamline plot, Fig. 3, in the first part of this study (Robinson *et al.*, 1996)). Because it is derived from the analytical model, which assumes one-dimensional flow, our definition for the capacitance does not account for adjustments in the size of the region from which the basement draws soil gas due to the addition of a gravel layer. However, Fig. 6 reveals that the analytical model predicts the volume of this region to within a factor 2.

Soil-gas and contaminant entry driven by typical atmospheric pressure fluctuations

Table 2 lists values of Q_{RMS} calculated by combining predictions of the numerical model with the long-term estimate of f_{dp} shown in Fig. 3b. These results reveal how changes in soil properties, water table depth, and the presence or absence of an impermeable floor slab affect Q_{RMS}. As noted earlier, Q_{RMS} describes the rate at which gas is pumped into and out of a basement in response to typical changes in atmospheric pressure.

Table 2 shows that increasing the permeability of the soil block three orders of magnitude from 10^{-13} to 10^{-10} m^2 only increases Q_{RMS} by a factor of ~6 (case 1). In contrast, a more linear relationship exists between Q_{RMS} and both air-filled porosity and water table depth (cases 2 and 3). For all cases, removing the concrete slab

increases Q_{RMS} by more than a factor of 3.5. However, the presence or absence of a concrete slab does not alter the relative relationship between Q_{RMS} and the permeability, porosity, and water table depth. For example, Q_{RMS} scales nearly linearly with air-filled porosity in both a basement with and without the floor slab.

For comparison, the values of steady-state soil-gas entry rate driven by a steady 1 Pa indoor-outdoor pressure difference, Q_{SS}, are also listed in Table 2. An examination of these values reveals that Q_{SS} varies linearly with soil permeability (case 1), depends slightly on water table depth (case 3), and is independent of air-filled porosity (case 2). In comparison, the relationship between Q_{RMS} and these properties is much more complex. Q_{RMS} varies non-linearly with soil permeability, linearly with porosity, and nearly linearly with water table depth.

Fundamentally, soil-gas flow driven by atmospheric pressure changes depends on the characteristic response time and the capacitance of the soil. In Fig. 8, we have plotted Q_{RMS} as a function of the characteristic response time for several different values of soil capacitance. These results were calculated using eqn. (8) and the long-term estimate of f_{dp} shown in Fig. 3b. The analytical model was used for this analysis because use of the numerical model would have required an enormous amount of computation time to evaluate so many different combinations of soil properties and water table depths. A comparison between the predictions of the analytical model and finite element model indicates that the analytical model correctly predicts the relationship between Q_{RMS}, the characteristic response time, and the capacitance of the soil. For the cases listed in Table 2, the values of Q_{RMS} calculated with the analytical model are within a factor of 2 of those based on predictions of the finite element model.

Fig. 8 reveals two important characteristics of soil-gas flow driven by atmospheric pressure fluctuations. First, the largest values of Q_{RMS} occur in buildings surrounded by soils with short characteristic response times and large soil capacitance. Second, Q_{RMS} is relatively insensitive to changes in τ if this response time is less than ~ 1000 s because more than 60% of the total power of the long-term time-rate-of-change of typical atmospheric pressure fluctuations occurs at frequencies less than 100 day^{-1}.

Using Q_{RMS} as a surrogate for the contaminant entry rate, the results presented in Table 2 and Fig. 8 provide insight into the influence of soil properties, water table depth, and a subslab gravel layer on contaminant entry driven by atmospheric pressure fluctuations. These results suggest that the largest contaminant entry rate driven by atmospheric pressure fluctuations will likely occur in a basement with a high-permeability subslab gravel layer surrounded by a soil with a short characteristic response time and a large capacitance. To possess these qualities a soil must have both a high permeability and a large air-filled porosity; the texture of such a soil might be described as sandy (USDA, 1975; Nielson and Rogers, 1990).

In addition to maximizing contaminant entry driven by atmospheric pressure fluctuations, a high-permeability soil will also maximize the entry rate driven by steady indoor-outdoor pressure differences. For such a soil, the results in Table 2 suggest that indoor-outdoor pressure differences will drive a much larger fraction of the total

contaminant entry rate than atmospheric pressure fluctuations (case 1, $k = 10^{-10}$ m^2). However, these results also suggest that contaminant entry driven by typical atmospheric pressure fluctuations will likely be relatively more important than contaminant entry in a basement surrounded by a less permeable soil with a large capacitance. For example, a plot of case 1 shown in Fig. 9 illustrates how the non-linear relationship between Q_{RMS} and permeability affects the relative importance of contaminant entry driven by these two different mechanisms. Because of this non-linear relationship, Q_{RMS} and Q_{SS} intersect at a soil permeability of ~ 10^{-12} m^2. The texture of a less permeable soil with high porosity might be described as clayey (USDA, 1975; Nielson and Rogers, 1990).

Our estimates of contaminant entry based on Q_{RMS} are consistent with the calculations of radon entry driven sinusoidal oscillations of atmospheric pressure previously reported by Tsang and Narasimhan (Tsang and Narasimhan, 1992). Our work has examined these effects in greater detail and provides additional physical insight into the phenomenon.

CONCLUSIONS

We have investigated the effects of atmospheric pressure fluctuations on soil-gas entry into houses. Because atmospheric pressure fluctuations can draw soil gas into a basement without the indoor-outdoor pressure differences commonly associated with the advective transport of radon and other soil-gas contaminants into houses, soil-gas flow driven by these fluctuations may represent an important mechanism for the transport of contaminants into houses.

Soil-gas flow driven by atmospheric pressure fluctuations can be described in terms of the characteristic response time and the capacitance of the soil. The response time characterizes the relaxation time of the soil gas to a change in atmospheric pressure, while the capacitance describes the volumetric change of the soil gas in response to a change in atmospheric pressure. If the period of an atmospheric pressure fluctuations is much longer than the characteristic response time, then the gas flow rate into and out of the depends only on the capacitance of the soil. As the period of these pressure fluctuation approach the characteristic response time of the soil, this response time restricts the gas flow rate into and out of the basement. Consequently, the shorter the characteristic response time and the larger the capacitance of the soil, the larger the gas flow rate into and out of building caused by a given change in atmospheric pressure.

Although atmospheric pressure fluctuations occur over a wide range of frequencies and magnitudes, relatively low-frequency (< 100 day^{-1}) oscillations in atmospheric pressure are the most important for driving long-term soil-gas entry into houses. The finite response time of the soil gas to a change in pressure restricts the entry caused high-frequency changes in atmospheric pressure. In addition, more than 60% of the total power of the time-rate-of-change of typical atmospheric pressure fluctuations occurs at frequencies less than 100 day^{-1}.

The presence of a high permeability subslab gravel layer can increase the soil-gas flow rate into a basement driven by atmospheric pressure fluctuations by more than a factor of 3. The size of this increase largely depends on

the ratio of the permeability of the gravel to that of the rest of the soil. If the permeability of the gravel is 2 orders of magnitude larger than the rest of the soil, a basement with a small perimeter crack and a subslab gravel layer effectively acts as if it has an open dirt floor.

Although the dilution of the soil-gas underneath a basement slab by the outflow of indoor air driven by rising atmospheric pressure complicates the analysis of the contaminant entry rate, the results of this study suggest the maximum contaminant entry rate driven by atmospheric pressure fluctuations will occur into a basement with a high permeability subslab gravel layer surrounded by a high permeability soil with a large air-filled porosity. Relative to entry driven by steady indoor-outdoor pressure differences, contaminant entry driven by atmospheric pressure will likely be most important in houses surrounded by soil with low permeabilities and a large air-filled porosity.

ACKNOWLEDGMENTS

We thank M. Fischer, R. Greif, W. Nazaroff, and S. Schery for their critical reviews of this manuscript and J. Li and Y. Tsang for suggesting this application of RN3D. This work was supported by the Director, Office of Energy Research, Office of Health and Environmental Research, Environmental Sciences Division, and by the Assistant Secretary for Energy Efficiency and Renewable Energy, Office of Building Technology of the U.S. Department of Energy (DOE), under Contract DE-AC03-763SF00098.

REFERENCES

Bear J. (1972) *Dynamics of Fluids in Porous Media.* Dover Publications Inc., New York.

Bendat J. S. and Piersol A. G. (1986) *Random data: analysis and measurement procedures.* Wiley-Interscience, New York.

Chatfield C. (1989) *The analysis of time series: an introduction.* Chapman and Hall, London.

Fisk W. J., Modera M. P., Sextro R. G., Garbesi K., Wollenberg H. A., Narasimhan T. N., Nuzum T. and Tsang Y. W. (1992) Radon entry into basements: approach, experimental structures, and instrumentation of the small structures project. LBL-31864, Lawrence Berkeley National Laboratory, Berkeley CA 94720.

Garbesi K., Sextro R. G., Fisk W. J., Modera M. P. and Revzan K. L. (1993) Soil-gas entry into an experimental basement: Model-measurement comparisons and seasonal effects. *Environ. Sci. Technol.* **27**, 466-473.

Gossard E. E. (1960) Spectra of atmospheric scalars. *J. Geophys. Res.* **65**, 3339-3351.

Gossard E. E. and Hooke W. H. (1975) *Waves in the atmosphere: atmospheric infrasound and gravity waves -- their generation and propagation.* Elsevier, New York.

Hodgson A. T., Garbesi K., Sextro R. G. and Daisey J. M. (1992) Soil-gas contamination and entry of volatile organic compounds into a house near a landfill. *J. Air Waste Mange. Assoc.* **42**, 277-283.

Holford D. J. (1994) RN3D: A finite element code for simulating gas flow and radon transport in variably saturated, nonisothermal porous media: user's manual, version 1.0. PNL-8943, Pacific Northwest Laboratory, Richland WA 99352.

Little J. C., Daisey J. M. and Nazaroff W. W. (1992) Transport of subsurface contaminants into buildings: An exposure pathway for volatile organics. *Environ. Sci. Technol.* **26**, 2058-2066.

Narasimhan T. N., Tsang Y. W. and Holman H. Y. (1990) On the potential importance of transient air flow in advective radon entry into buildings. *Geophysical Research Letters* **17**, 821-824.

Nazaroff W. W. (1992) Radon transport from soil to air. *Review of Geophysics* **30**, 137-160.

Nielson K. K. and Rogers V. C. (1990) Radon transport properties of soil classes for estimating indoor radon entry. Published in the Proceedings of Twenty-Ninth Hanford Symposium on Health and the Environment: *Indoor Radon and Lung Cancer: Reality of Myth?* Pacific Northwest Laboratory, Richland WA, Battelle Press.

Revzan K. and Fisk W. (1992) Modeling radon entry into houses with basements: The influence of structural factors. *Indoor Air* **2**, 40-48.

Revzan K. L., Fisk W. J. and Gadgil A. J. (1991) Modeling radon entry into houses with basements: Model description and verification. *Indoor Air* **1**, 173-189.

Robinson A. L. and Sextro R. G. (1995a) Direct measurements of soil-gas entry into an experimental basement driven by atmospheric pressure fluctuations. *Geophysical Research Letters* **22**, 1929-1932.

Robinson A. L. and Sextro R. G. (1995b) The influence of a subslab gravel layer and open area on soil-gas and radon entry into two experimental basements. *Health Phys.* **69**, 367-377.

Robinson A. L., Sextro R. G. and Fisk W. J. (1996) Soil-gas entry into houses driven by atmospheric pressure fluctuations, part 1 --- Measurements, spectral analysis, and model comparison. LBL-38232, Lawrence Berkeley Laboratory, Berkeley CA 94720.

Scott A. G. (1988) Preventing radon entry. In Nazaroff W. W. and Nero A. V. (Ed.) *Radon and Its Decay Products in Indoor Air*, John Wiley and Sons, New York, N.Y., 407-433.

Tsang Y. W. and Narasimhan T. N. (1992) Effects of periodic atmospheric pressure variation on radon entry into buildings. *J. Geophys. Res.* **97**, 9161-9170.

USDA (1975) *Soil taxonomy*. U.S. Department of Agriculture, Soil Conservation Service, Washington D.C.

NOMENCLATURE

A	Vertical cross sectional area of gravel layer or dirt floor (m^2)
arg( )	Argument of a complex number (-)
C	Capacitance of soil-structure system ($m^3\ Pa^{-1}$)
D_p	Pressure diffusivity of soil ($m^2\ s^{-1}$) : $D_p = \frac{k\overline{P}}{\varepsilon\mu}$
$f_{dp}(\omega)$	Time-rate-of-change of atmospheric pressure power spectrum ($Pa^2\ s^{-1}$)
$f_p(\omega)$	Atmospheric pressure power spectrum ($Pa^2\ s$)
$f_q(\omega)$	Soil-gas flow power spectrum ($m^6\ s^{-1}$)
$G_{q,dp}(\omega)$	Gain function, amplitude of q(t) caused by a 1 Pa s^{-1} oscillation in the time-rate-of-change in atmospheric pressure ($m^3\ Pa^{-1}$)
i	$\sqrt{-1}$
k	Soil permeability to gas flow (m^2)
L	Depth of the water table below the gravel layer or dirt floor (m)
n	Index for infinite summation (-)
$\overline{P}$	Mean soil-gas pressure (Pa)
$P(t)$	Atmospheric pressure (Pa)
$P'(t)$	Time derivative of atmospheric pressure (Pa s^{-1})
$q(t)$	Gas flow rate into and out of a basement driven by fluctuations in atmospheric pressure ($m^3\ s^{-1}$)
Q_{RMS}	Root-mean-square soil-gas entry rate ($m^3\ s^{-1}$)
$Q_{step}(t)$	Step response function, soil-gas flow into a house in response to 1 Pa step change in atmospheric pressure ($m^3\ s^{-1}\ Pa^{-1}$)
R	Resistance of soil to gas flow (Pa s m^{-3})
t	Time (s)
T	Period over which a time average is taken (s)
T_n	Time for index n (s)
$\chi(\omega)$	Frequency response function ($m^3\ Pa^{-1}$)
$\chi_a(\omega)$	Frequency response function predicted by analytical model ($m^3\ Pa^{-1}$)
ε	Air-filled porosity (-)
$\phi_{q,dp}(\omega)$	Phase function, phase shift between q(t) and oscillations in the time-rate-of-change of atmospheric pressure (radians)
μ	Dynamic viscosity of soil-gas (Pa s)
θ	Dummy variable used to integrate over time (s)
τ	Characteristic response time of soil gas to a change in atmospheric pressure (s)
ω	Circular frequency (radians s^{-1})
$\lvert\ \rvert$	Modulus of a complex number (-)

Table 1. Soil properties used for simulations shown in Figs. 4 and 5.

Fig.	k (m^2)	ε (-)	L (m)[a]	τ (s)[b]	C (L Pa^{-1})[c]
4c, 5a, 5b, 5c	10^{-11}	0.4	8	~ 460 s	2.50
4c, 5a, 5c	5×10^{-12}	0.2	8	~ 460 s	1.25
4d, 5b, 5c	10^{-10}	0.4	8	~ 46 s	2.50
4d, 5b, 5c	10^{-12}	0.4	8	~ 4,600 s	2.50

[a] L = distance between basement floor and water table
[b] calculated with $\overline{P}$ = 100,000 Pa, and $\mu = 1.8 \times 10^{-5}$ Pa
[c] calculated with $\overline{P}$ = 100,000 Pa, and A = 78.5 m^2

Table 2. Soil properties used for simulations shown in Figs. 7 and 8. Calculated soil-gas entry rate, Q_{SS}, driven by a 1 Pa steady indoor-outdoor pressure difference, and the root-mean-square soil-gas entry rate, Q_{RMS}, caused by typical atmospheric pressure fluctuations.

case	k (m^2)	ε (-)	L (m)[a]	τ (s)[b]	C (L Pa^{-1})[c]	Dirt Floor		Perimeter Crack	
						Q_{SS} (L min^{-1})	Q_{RMS} (L min^{-1})	Q_{SS} (L min^{-1})	Q_{RMS} (L min^{-1})
1	10^{-10}	0.4	8	46	2.5	8.6	0.53	2.7	0.14
1	10^{-11}	0.4	8	460	2.5	0.86	0.34	0.27	0.091
1	10^{-12}	0.4	8	4,600	2.5	0.086	0.20	0.027	0.052
1	10^{-13}	0.4	8	46,000	2.5	0.0086	0.088	0.0027	0.021
2	10^{-11}	0.2	8	230	1.25	0.86	0.20	0.27	0.055
2	10^{-11}	0.3	8	345	1.9	0.86	0.28	0.27	0.074
2	10^{-11}	0.4	8	460	2.5	0.86	0.34	0.27	0.091
2	10^{-11}	0.5	8	575	3.1	0.86	0.41	0.27	0.11
3	10^{-11}	0.4	3	65	0.9	0.70	0.18	0.25	0.053
3	10^{-11}	0.4	8	460	2.5	0.86	0.34	0.27	0.091
3	10^{-11}	0.4	13	1,220	4.1	0.88	0.45	0.27	0.12
3	10^{-11}	0.4	18	2,330	5.7	0.89	0.54	0.27	0.14

[a] L distance between basement floor and water table
[b] calculated with $\overline{P}$ = 100,000 Pa, and $\mu = 1.8 \times 10^{-5}$ Pa s
[c] calculated with $\overline{P}$ = 100,000 Pa, and A = 78.5 m^2

a

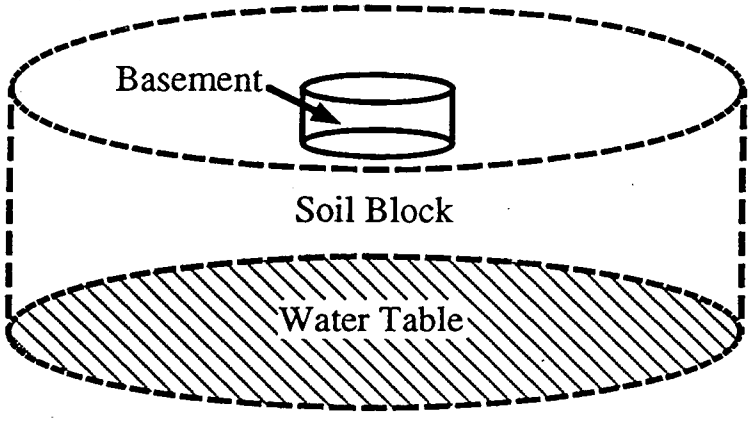

b

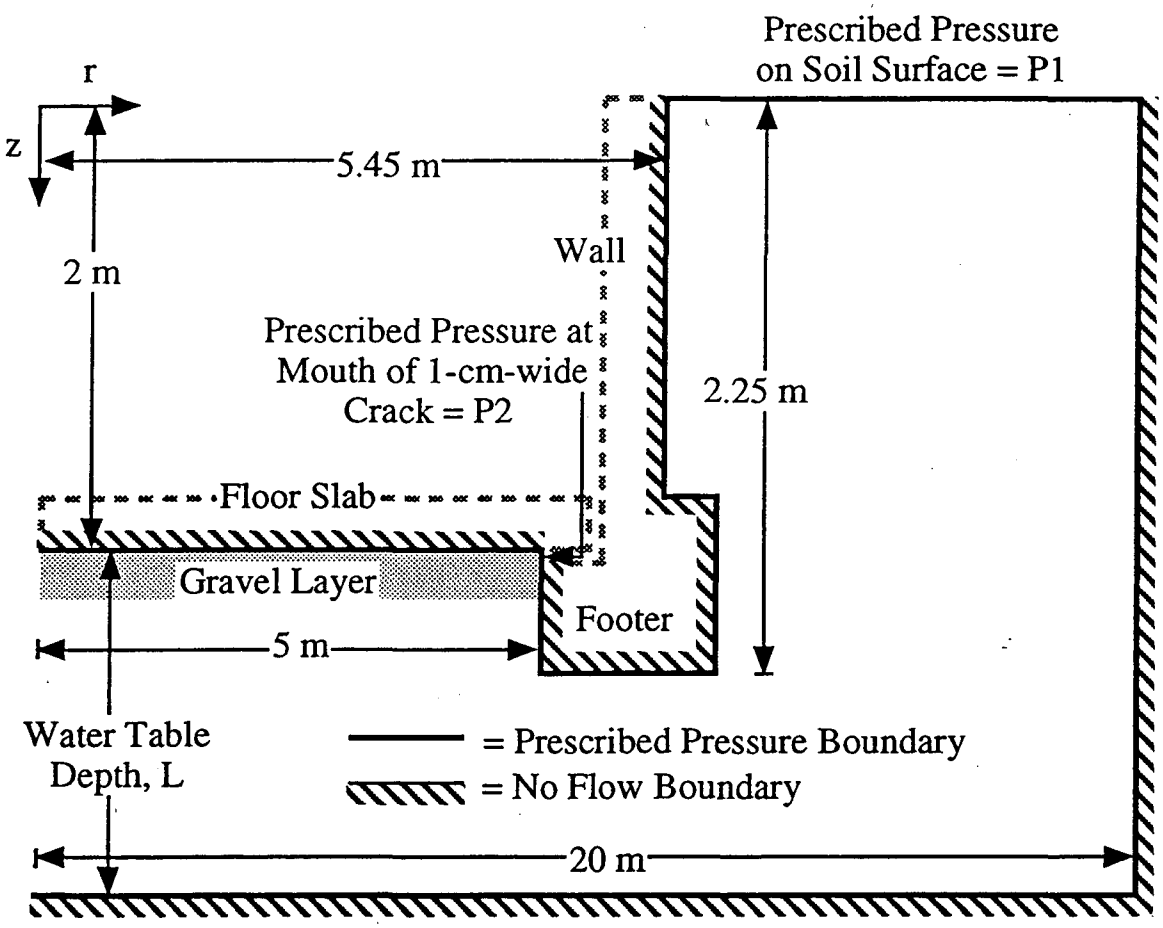

Fig. 1 Schematic of: (a) the cylindrical basement and soil block; (b) cross-section of model basement and soil block (due to axial-symmetry only half the cylinder is shown). The finite-element model calculates the soil-gas pressure and velocity inside the region bound by the heavy black line shown in Fig. (b). The dashed lines indicate the interior edges of the walls of the structure. These lines are intended for visual guidance only. Only the gravel layer with a perimeter gap configuration is shown in (b). For simulations of a basement with an open dirt floor the gravel layer is assigned the same properties as the rest of the soil block and the prescribed pressure boundary condition P2 is applied across the bottom of the entire floor slab. For simulations of a basement with a perimeter gap and a homogeneous soil block the gravel layer is assigned the same properties as the rest of the soil block. The figure is not drawn to scale.

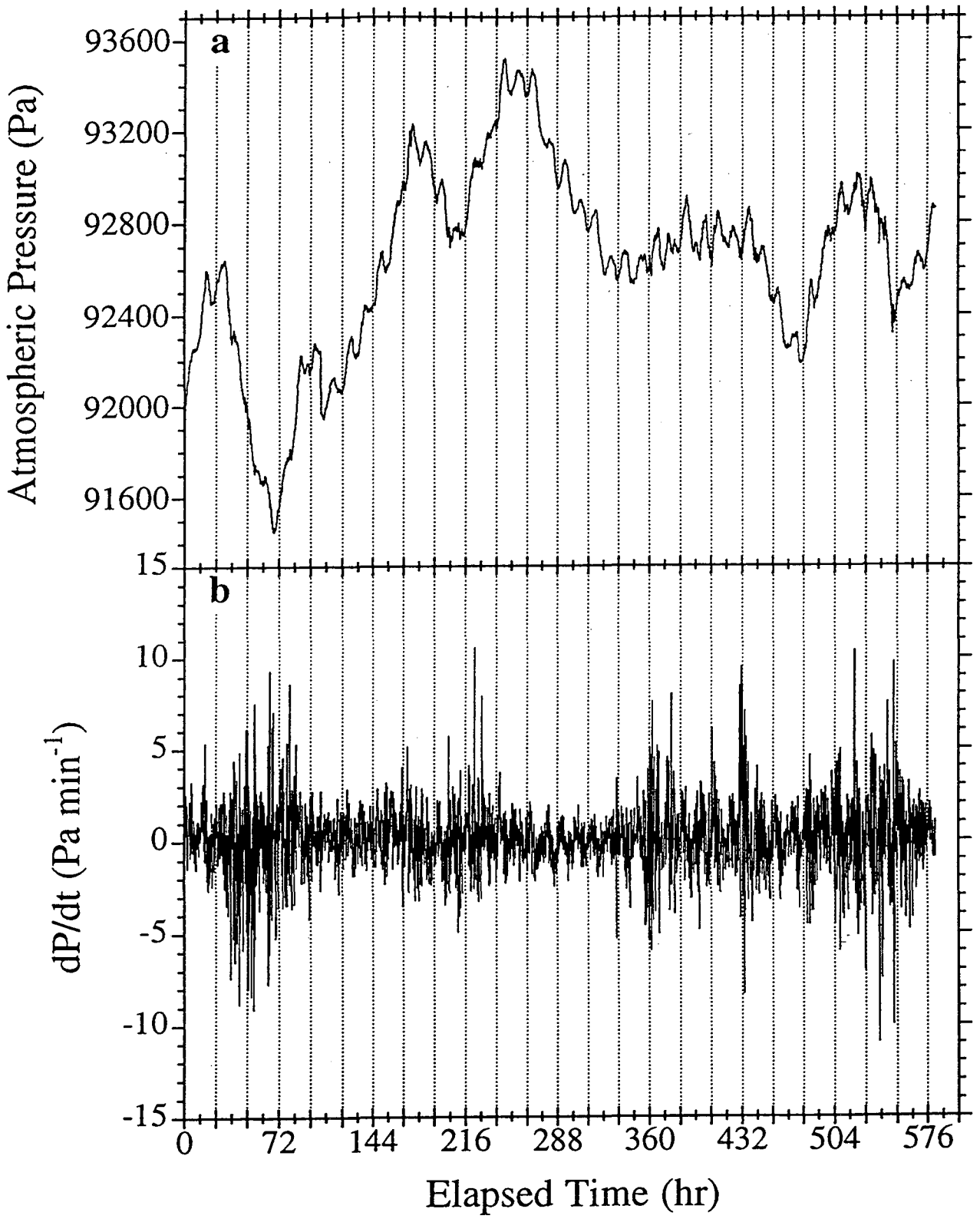

Fig. 2 (a) Atmospheric pressure measured during a 24-day experiment; (b) time-rate-of-change of atmospheric pressure, defined as the change in pressure over a two-minute time interval. These data were collected during the February and March of 1993.

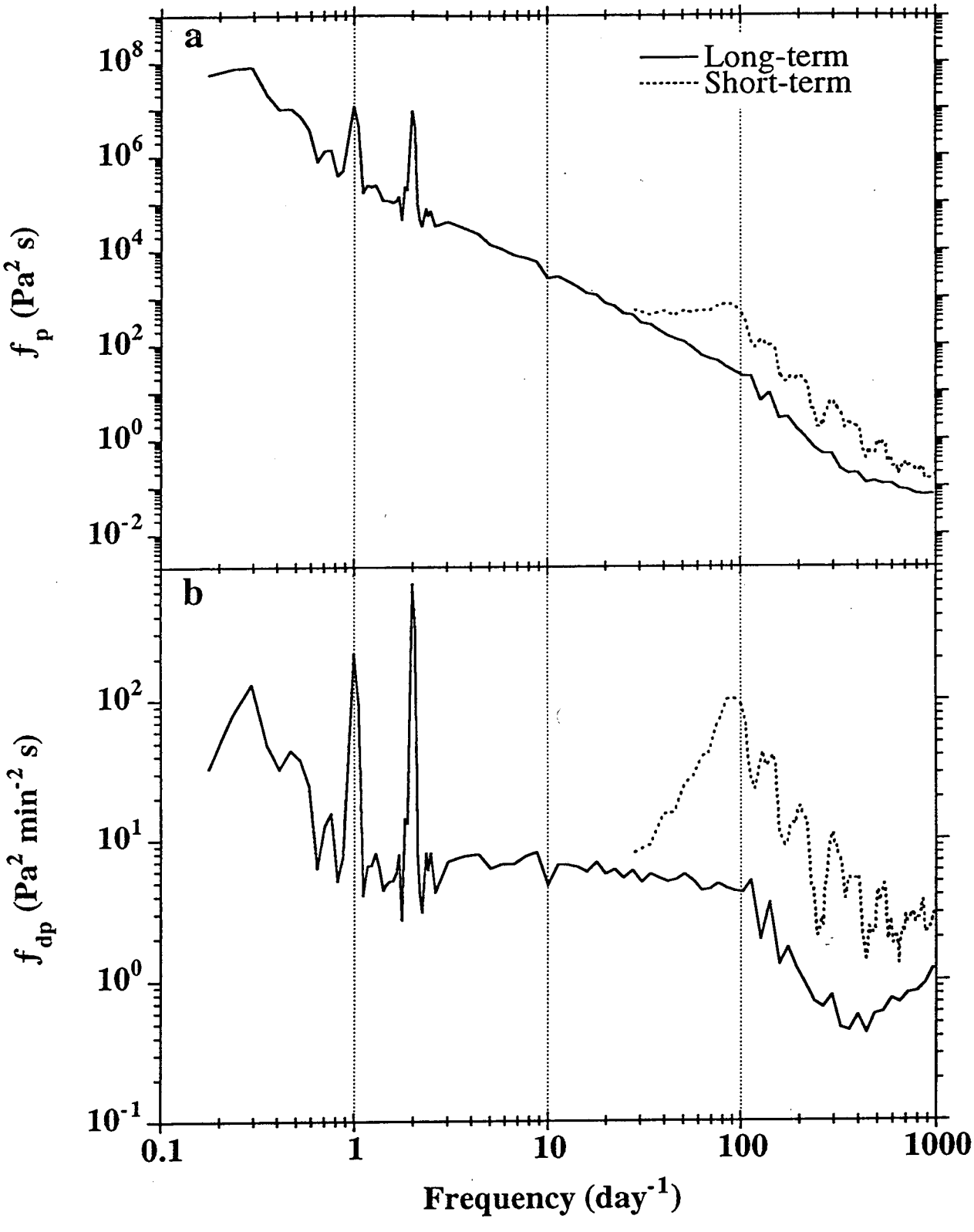

Fig. 3 Power spectra for: (a) atmospheric pressure; (b) time-rate-of-change of atmospheric pressure. The long-term spectra are based on more than 108 days of measured atmospheric pressure data, while the short-term spectra are based on 5 hours of data.

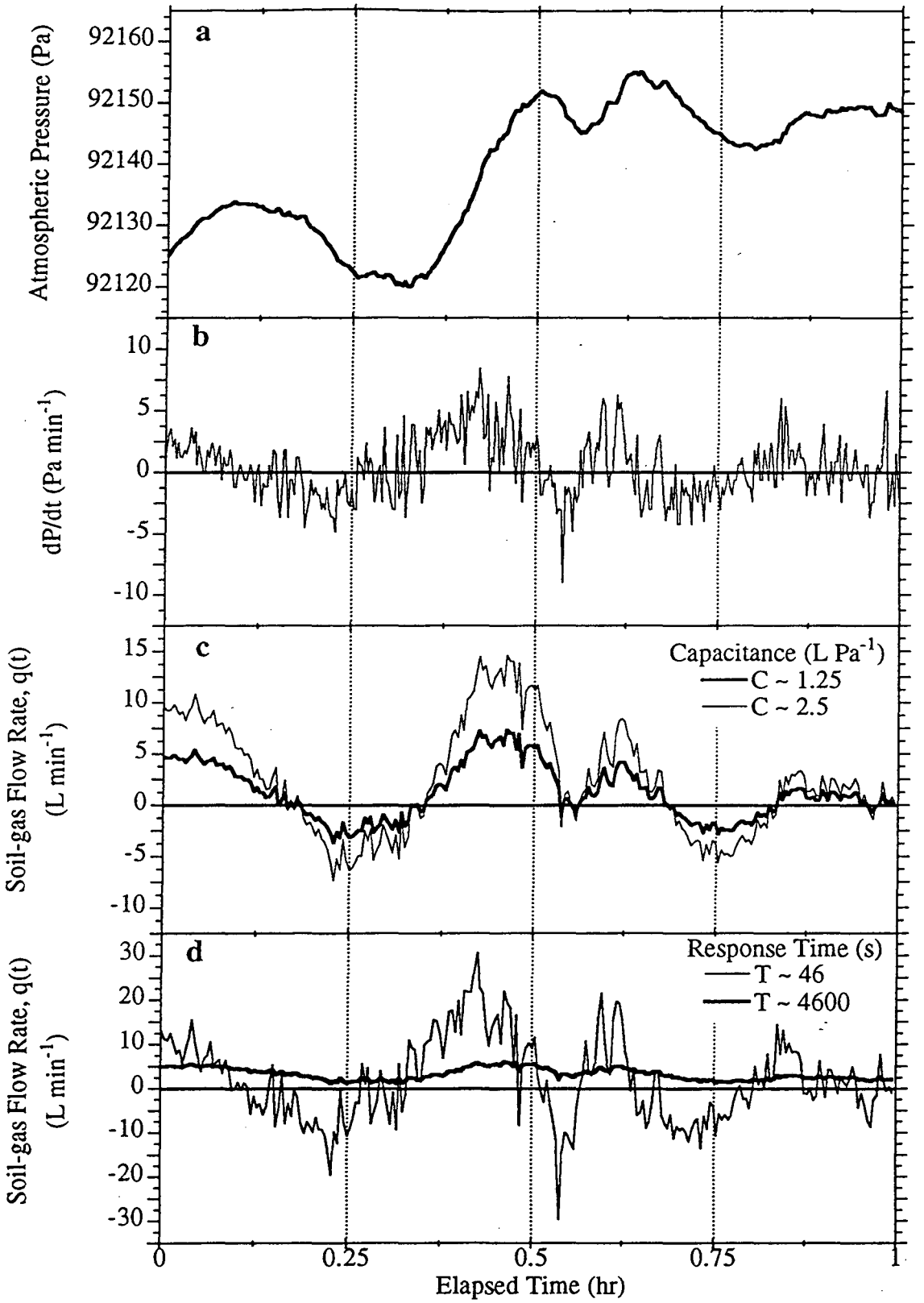

Fig. 4 Atmospheric pressure and calculated gas flow into and out of a basement with a dirt floor: (a) measured atmospheric pressure used as boundary condition for calculations; (b) time-rate-of-change in atmospheric pressure, defined as the change in pressure over a 15-s interval; (c) q(t) as a function of capacitance with the characteristic response time held constant (τ ~ 460 s); (d) q(t) as function of characteristic response time with the capacitance held constant (C ~ 2.5 L Pa^{-1}). Negative flow rates indicate entry into the basement. Soil properties used for these calculations are listed in Table 1.

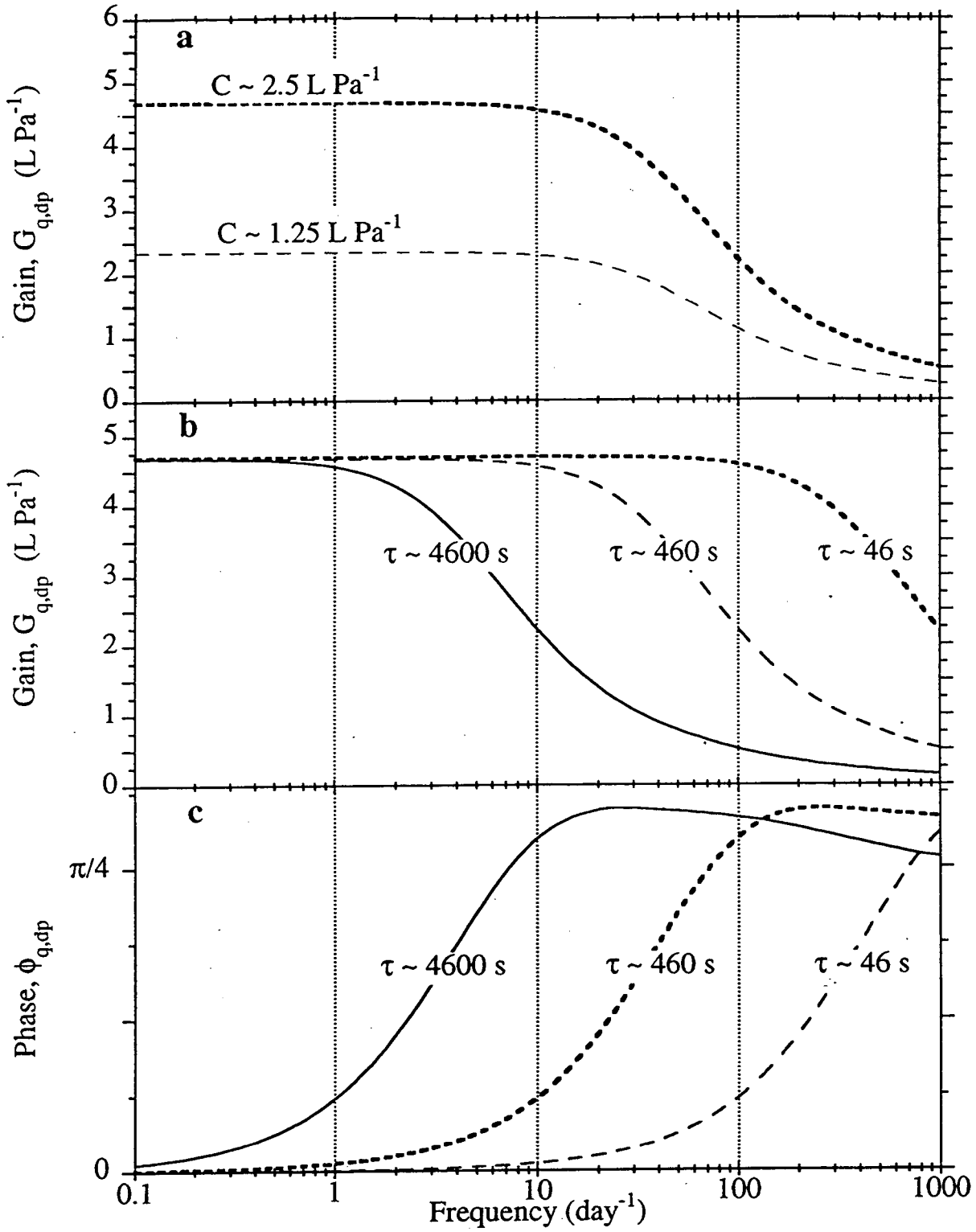

Fig. 5 Calculated frequency response function for a basement with a dirt floor: (a) gain, $G_{q,dp}(\omega)$, as a function of capacitance with the characteristic response time held constant ($\tau \sim 460$ s); (b) gain, $G_{q,dp}(\omega)$, as a function of characteristic response time with the capacitance held constant (C ~ 2.5 L Pa^{-1}); (c) phase function, $\phi_{q,dp}(\omega)$. Soil properties are listed in Table 1.

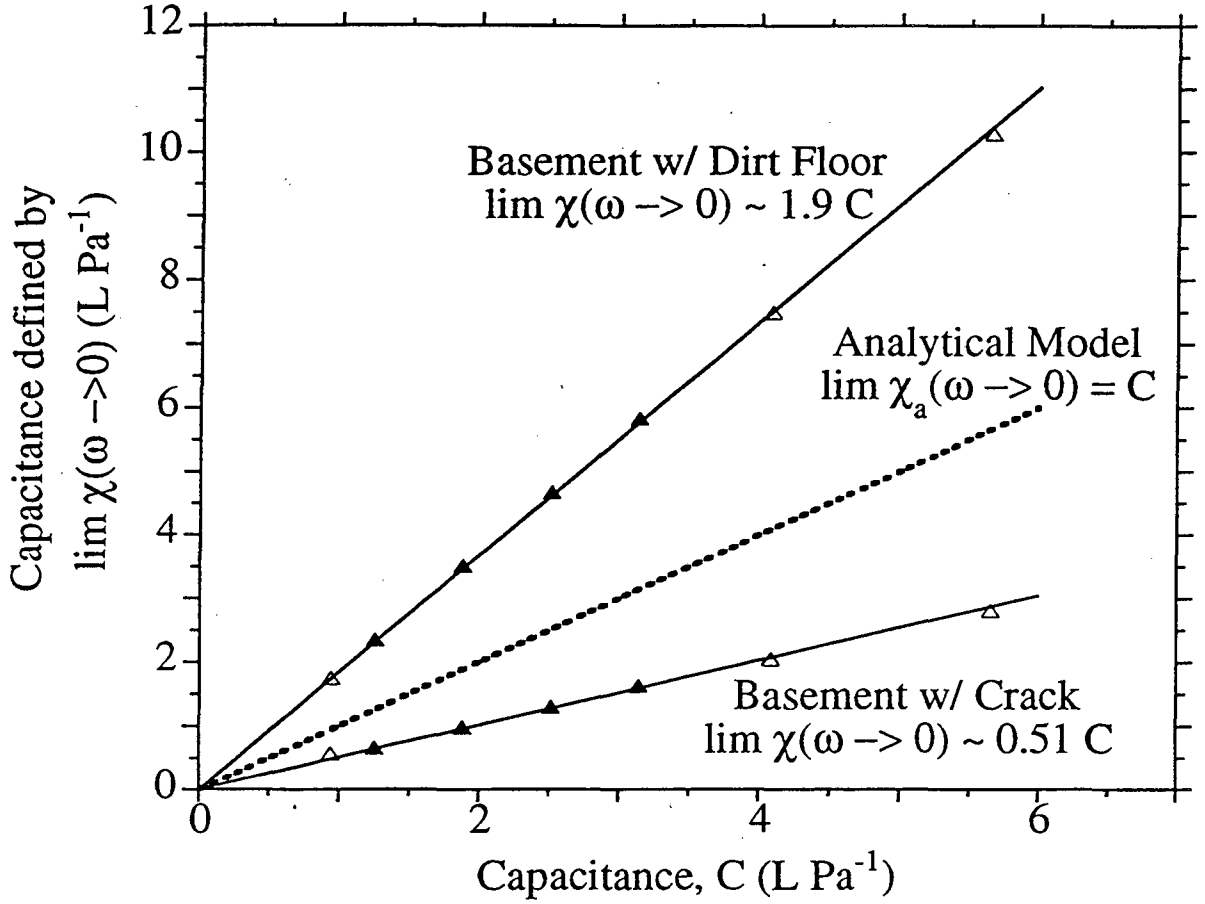

Fig. 6 Low-frequency limit of $\chi(\omega)$ as a function of the capacitance. The capacitance is varied by changing either the water table depth while holding the air-filled porosity fixed at 0.4 (open symbols) or the air-filled porosity while holding the water table depth fixed at 8 m (solid symbols). The values of the soil properties used for these calculations are listed as cases 2 and 3 in Table 2. Solid lines indicate linear regressions, where $R^2 > 0.999$ in each case. The dashed line indicates low frequency limit of $\chi_a(\omega)$ defined by the analytical model.

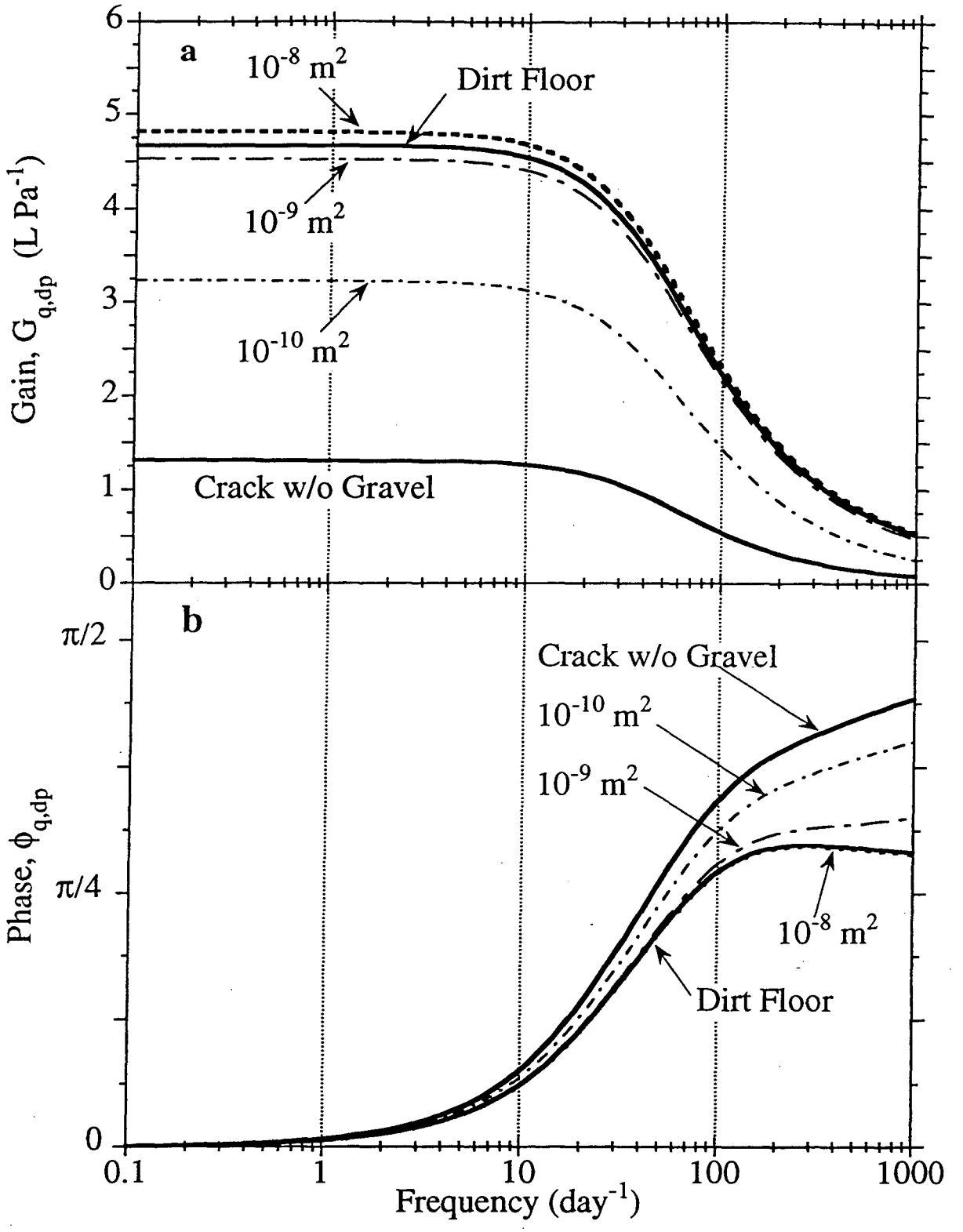

Fig. 7 Comparison of the frequency response function for a basement with a dirt floor and a basement with a perimeter crack: (a) gain, $G_{q,dp}(\omega)$; (b) phase, $\phi_{q,dp}(\omega)$. For the basement with a perimeter crack, the permeability of a 10-cm-thick gravel layer immediately underneath the slab was varied between 10^{-10} and 10^{-8} m^2. Numbers labeling curves indicate permeability of gravel layer. Other properties used for these simulations are: water table depth L = 8 m, permeability of the soil (not including gravel layer) k = 10^{-11} m^2, air-filled porosity of the soil (not including gravel layer) $\varepsilon = 0.4$.

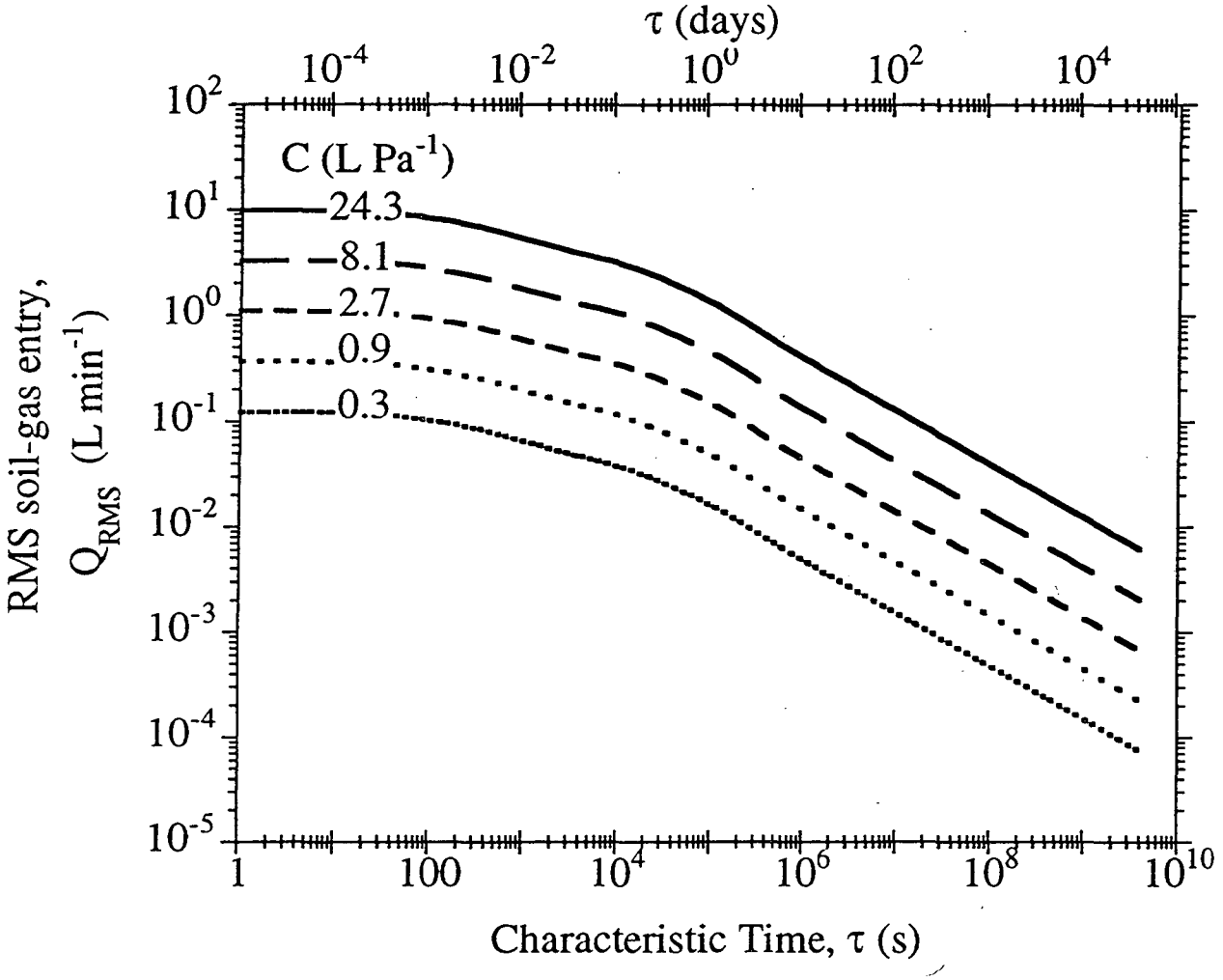

Fig. 8 Q_{RMS} as a function of characteristic response time and capacitance. For this analysis, we employed eqn. (8) and long-term spectrum shown in Fig. 3b.

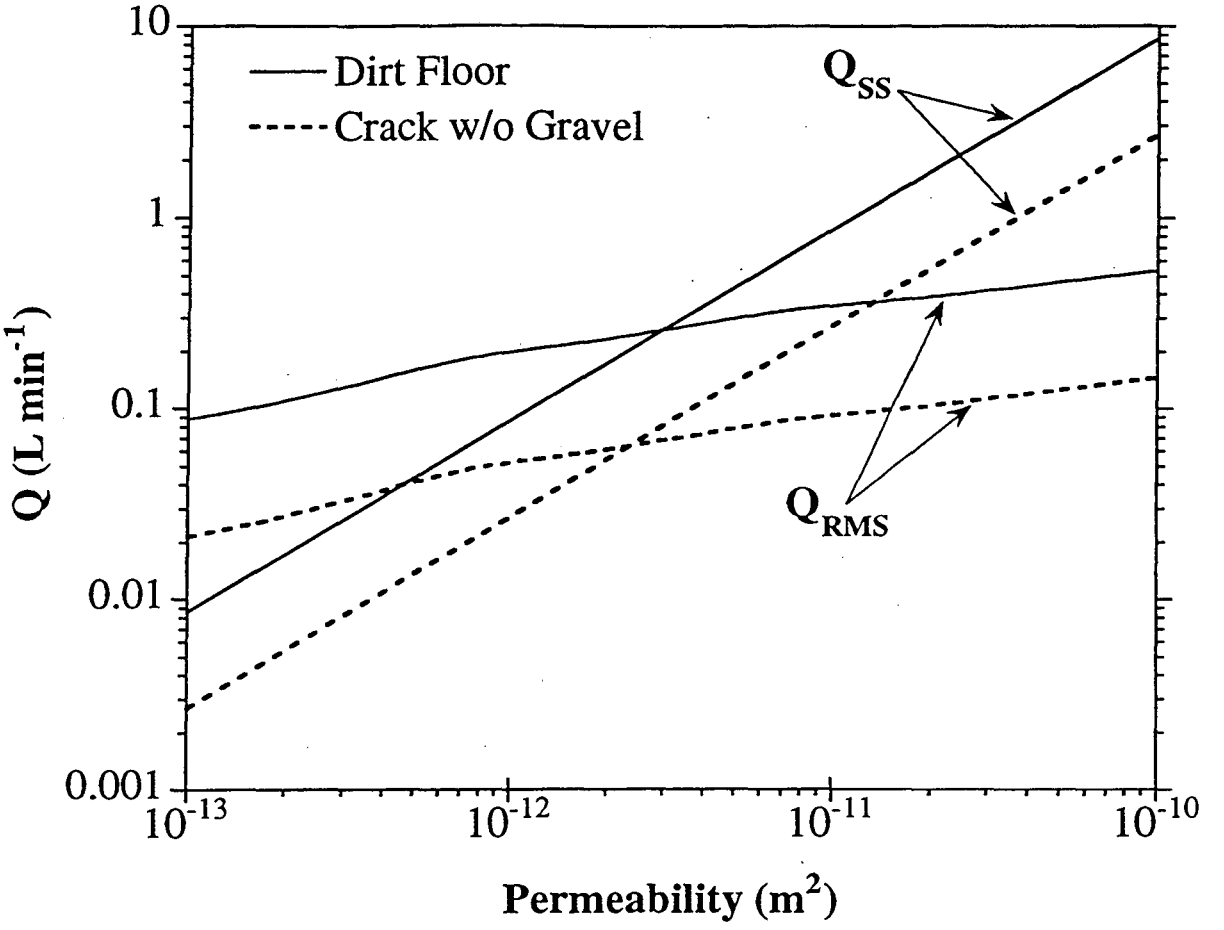

Fig. 9 Q_{RMS} and Q_{SS} as a function of soil permeability. Soil properties used for these simulations listed as case 1 in Table 2.

LAWRENCE BERKELEY NATIONAL LABORATORY
UNIVERSITY OF CALIFORNIA
TECHNICAL & ELECTRONIC INFORMATION DEPARTMENT
BERKELEY, CALIFORNIA 94720